JOURNAL OF MATERIALS SCIENCE 32 (1997) 3227–3235

Microstructural control by spray forming and wear characteristics of a Babbit alloy

A. UPADHYAYA
The Powder Metallurgy Laboratory, Pennsylvania State University, University Park, PA 16802-6809, USA

N. S. MISHRA
Research and Development Centre, Steel Authority of India Ltd., Ranchi-834002, India

S. N. OJHA
Department of Metallurgical Engineering, Banaras Hindu University, Varanasi-221 005, India

The effect of process variables during spray forming of a commercial Babbit alloy containing Pb74–Sn12–Sb11.5–Cu1.25–NiO.75–Cd0.3–As0.2 on its microstructure and wear characteristics were investigated. Variation in atomization gas pressure from 0.6 to 1.2 MPa and nozzle to substrate distance from 0.2 to 0.4 m revealed considerable change in the nature of porosity and microstructural features of the spray deposits. The process variables during spray deposition were optimized to achieve microstructural homogeneity and refinement in second phase particles of this alloy. The wear study of both the spray formed and as-cast alloy under an applied load of 10 to 70 N and sliding velocity of 0.2 to 1.5 ms^{-1} indicated two distinct regimes of mild and severe wear. In both the regimes, the spray-formed alloy consistently indicated a low wear rate compared to that of the as-cast alloy. In addition, the mild wear regime of the spray-formed alloy was extended to higher load and sliding velocity. Wear characteristics of the spray formed alloy is discussed in light of its microstructural features induced during spray deposition processing.

1. Introduction

Currently, lead-base Babbit alloys find extensive applications as bush bearing materials due to their antifriction property. These alloys are produced by the conventional casting method and their microstructure contains a dispersion of coarse intermetallic compounds in a pseudo-eutectic matrix. The microstructural control exercised during spray deposition processing of these alloys provides an exciting new opportunity for the development of materials with a superior wear property. In this process, a stream of molten metal is atomized by high-energy gas jets into a spray of micron-sized droplets which are subsequently deposited over a conductive substrate to build up a high-density perform. Although the process was pioneered by Singer [1, 2] and others [3] in the early seventies, the scientific understanding of the microstructural evolution during a deposition process has been understood only recently [4–10]. Several benefits of this processing methodology are by now well established. Rapid solidification effects inherent in the spray deposition process due to high heat exchange rate at the droplet–gas interface and also on the deposition surface ensures considerable chemical and microstructural homogeneity of the perform [11]. In addition, formation of equiaxed grain morphology with dispersion of ultrafine second phase particles enable achievement of enhanced physical and mechanical properties of the materials [12–15].

The microstructural evolution during spray deposition depends in a complex way on the droplet dynamics and their thermal state on the deposition surface. These are controlled by process variables employed to atomize the melt, nozzle–substrate distance and design of spray nozzles [16, 17]. Mathematical modelling based on heat transfer analysis has been invariably used to suggest that the overall solid fraction in the spray arriving on the deposition surface is critical to control the microstructure and porosity of the preform [18–20]. Generally, too low a solid fraction in the spray results in splashing of the liquid from the deposition surface and formation of large size pores of the entrapped gases. In this case, the microstructure of the preform resembles a typical cast structure. Alternatively, an excess solid fraction in the spray generates a preform with a large number of pores due to insufficient liquid phase available to provide bonding of particles during solidification of the spray deposit. Such a preform requires secondary processing to reduce porosity and to achieve microstructural homogeneity of the alloy. Consequently, an optimum control of the process variables is greatly emphasized to derive the maximum benefits of this processing methodology. The present investigation is aimed in this direction.

0022–2461

A commercial Pb-base Babbit alloy has been spray formed under different processing conditions. The effect of atomization gas pressure and nozzle-to-substrate distance on the microstructure and porosity of the preform have been studied. The wear characteristics of the preform is reported and compared with that of the alloy produced by the conventional casting process.

2. Experimental details

2.1. Experimental procedure

The details of the spray forming set-up are described elsewhere [21]. In brief, the process employs an annular convergent–divergent nozzle, with a throat area of 20.5 mm^2 and exit-to-throat area ratio of 2.5 : 1, for atomization of the melt. In this process, the gas interacts with the melt stream at the tip of a flow tube concentric with the gas flow channel as shown in Fig. 1. The resultant spray of droplets is deposited on a copper substrate in an environmental chamber.

The composition of the alloy is given in Table I. In each experiment 2.5 kg of the alloy was charged in a graphite bonded fireclay crucible. The melting was carried out in a resistance heating furnace under argon atmosphere. The temperature of the melt was measured using a chromel–alumel thermocouple connected to a temperature recorder. A melt superheat of 300 K was ensured to stop the premature freezing of the melt. The detail of the process variables are listed in Table II. The melt was atomized by N_2 gas at an atomization gas pressure varying from 0.6 to 1.2 MPa. The nozzle to substrate distance was varied from 0.2 to 0.4 m. The melt flow rate was obtained by the mass of the charge in the crucible and duration of atomization. The gas flow rate was estimated by laws of isentropic gas flow [22].

In another experiment, the substrate was removed and the melt was atomized to allow solidification of droplets during free flight in the environmental chamber. The powders were sieved into various size fractions and the sieve analysis data were plotted to obtain the median particle diameter (d_m) and standard deviation (σ) of the particle size distribution.

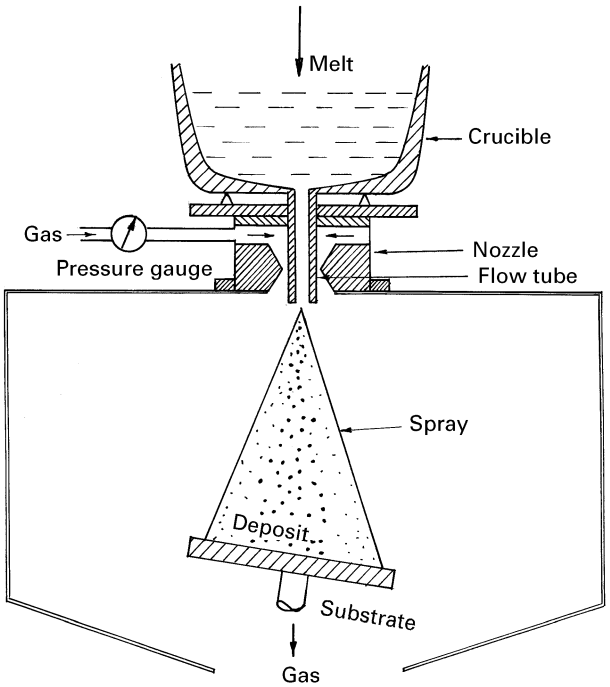

Figure 1 Schematic diagram of the spray forming set-up.

TABLE I Chemical composition of the alloy

Element	(wt %)
Pb	74
Sn	12
Sb	11.5
Cu	1.25
Ni	0.75
Cd	0.30
As	0.20

TABLE II Experimental variables in spray forming

Run	Gas pressure (MPa)	Nozzle–substrate distance (m)	Internal diameter of flow tube (mm)	Gas–metal flow ratio
1	0.8	0.4	4	0.60
2	1.0	0.4	4	0.68
3	1.2	0.4	4	0.74
4	1.2	0.3	3	1.22
5	1.2	0.2	3	1.20

2.2. Materials characterization

Several samples from the centre and peripheral regions of the spray deposit were prepared for microstructural examination and porosity measurements. These were polished using a standard metallographic procedure and etched with a 5% Nital solution. The microstructural examination was carried out in a Metallux-3 optical microscope. The size of the second phase particles was measured using a VIDS image analyser. The surface morphologies of the atomized powders were examined using a Jeol 840 CX scanning electron microscope operating at 15 kV. A qualitative analysis of the elemental distribution in the spray deposit, as well as in the alloy produced by conventional casting, was carried out using an electron probe microanalyser model Jeol JCXA 733 operating at 25 kV.

The spray deposition often generates open and closed porosity in the preform depending on the experimental parameters employed in materials processing [14]. Since a range of process conditions was used in the present work, it was necessary to evaluate their influence on the nature of porosity in different sections of the deposit. The porosity measurement was carried out on samples ($10 \times 10 \times 5$ mm^3) prepared from different regions of the preform by the vacuum xylene impregnation method as described by Arthur [23]. The technique involves immersing the specimen in xylene solution and evacuating the system to 0.2 mm Hg by a rotary pump so as to fill the open pores.

Subsequent porosity determination was done by the water displacement method.

2.3. Wear testing

The wear test was conducted using specimens of 8 mm diameter × 25 mm length on a pin-on-disc type wear testing machine. The special feature of the set-up is available elsewhere [15]. Basically it consisted of a high carbon–chromium steel disc, 150 mm in diameter, hardened and tempered to a hardness value of 58 R_C . The disc was mounted on a gear driven shaft connected to a variable speed d.c. motor. The test specimen was mounted at the tip of a calibrated spring loaded cylinder. The compression of the spring provided the load on the contact surface of the specimen. The linear wear rate was recorded on a micrometer dial gauge connected to the specimen holder. The flat surfaces of both the specimen and disc were polished to a surface finish of 0.3 μm before each test. The wear testing was carried out at an applied load of 10 to 70 N for a test duration of 15 min and a sliding velocity of 0.5 ms^{-1}. Similarly the sliding velocity of the disc was varied from 0.2 to 1.5 ms^{-1} at a constant applied load of 30 N. The volume wear rate was calculated by continuous displacement measurements. All the experiments were carried out under dry sliding conditions and data was recorded at room temperature.

3. Results and discussion

3.1. Spray characteristics

The sieve analysis data of atomized powders provide valuable information about the nature of droplet size distribution during spray deposition. The data generated for three different gas pressures are presented in Fig. 2. The result indicates that the size of the major fraction of droplets in the spray varies from 25 to 200 μm. In addition, the fraction of small size droplets increases with increasing atomization gas pressure. The effect of gas pressure on the median particle diameter and standard deviation of particle size distribution is shown in Table III. It is worthwhile to note that by increasing the atomization gas pressure from 0.8 to 1.2 MPa, the median particle diameter is reduced from 70 to 50 μm with a consequent decrease in the standard deviation of the particle size distribution from 2.2 to 1.7. The result indicates that an increase in the gas pressure generates a large velocity of the gas stream. Consequently the kinetic energy of the gas imparted on the melt stream promotes an efficient atomization of the liquid metal resulting in a narrow size range of particle size distribution in this mode of atomization.

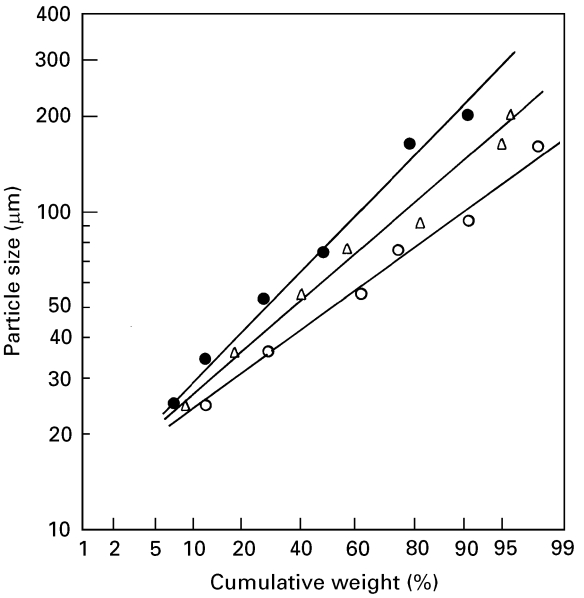

Figure 2 Variation in cummulative weight percentage with particle size of powders atomized at three different gas pressures. Gas pressure; ● 0.8 MPa; △ 1.0 MPa; ○ 1.2 MPa.

Knowledge of the droplet size distribution in the spray is essential in understanding the complex heat transfer and solidification phenomena in spray forming. Earlier investigations [24 –26] have shown that the primary break-up of liquid metal in an annular confined gas atomization process occurs by a prefilming mechanism. In this process the liquid metal runs at the tip of the flow tube and spreads into a thin film along the wall thickness of the tube. The thickness of the film depends on the melt flow rate and physical properties of the liquid [27]. The liquid film subsequently interacts with the high-velocity gas stream to promote atomization. The secondary disintegration of droplets then takes place in the high velocity gas field by bag break-up [28] or stripping [29] mechanisms depending on the relative velocity between the gas and the droplets. A small increase in the gas pressure and subsequent change in the velocity of the gas stream considerably influence the mode of break-up of liquid metal in this process. As a result, the characteristics of the spray have a strong dependence on the atomization gas pressure.

3.2. Porosity of the spray deposit

An important feature of the spray-formed alloy is the presence of a finite amount of porosity in the preform. The amount of porosity measured in different sections of the deposit is presented in Table IV. The total

TABLE III Effect of atomization gas pressure on the size and size distribution of particles

Run	Gas pressure (Mpa)	Stream diameter (mm)	Median particle diameter, d_m (μ_m)	Standard deviation (σ)	Specific surface area (m^2g^{-1})
6	0.8	4	70	2.2	0.0153
7	1.0	4	62	1.9	0.0163
8	1.2	4	50	1.7	0.0210

porosity (ε_t) constitutes the closed and inter-connected pores (ε_i) of the deposit. The result indicates that the spray deposition process variables have considerable influence on the formation of closed and interconnected porosity in the preform. The amount of closed porosity is invariably higher than the interconnected porosity and these are higher in the periphery of the preform compared to that at the centre. It should also be noted that a decrease in gas pressure and nozzle-to-substrate distance have similar effects on the control of the porosity during spray deposition. In addition, an increase in the gas-to-metal flow ratio tends to reduce the porosity of the perform. Many noteworthy observations are the variation in the size and shape of the pores in different regions of the spray deposits as shown in Fig. 3a and b. The size of the pores varies from 10 to 50 μm with large size pores having irregular shape. The large size pores are usually observed in the bottom and top sections of the preform whereas the central region depicts only small size pores. Similar observations were made in the preform of this alloy processed under different conditions with only marginal change in the size and distribution of porosity. For example large size pores are considerably reduced in Run no. 3 made at a higher gas pressure.

TABLE IV Effect of process variables on the amount of porosity of the spray deposit

Run	Porosity at centre		Porosity at the periphery	
	ε_t (%)	ε_i (%)	ε_t (%)	ε_i (%)
1	12	2	12	3
2	10	3	12	5
3	6	1	10	3
4	8	3	8	5
5	11	2	8	2

Several investigators [30, 31] have discussed the origin of porosity in the preform during spray deposition processing. The possible reasons for this effect are concerned with either gas entrapment or solidification shrinkage during the deposition process. In spray forming, the condition employing a small nozzle-to-substrate distance gives rise to an excessive liquid fraction on the deposition surface. Consequently high gas velocity causes whipping of the liquid and entrapment of gas leading to the formation of large size cavities. The irregular morphology of pores observed in the top region of the preform supports this mechanism of porosity formation. However, as the nozzle to substrate distance is increased for the same atomization gas pressure, the fraction of liquid decreases in the spray. The resultant preform in this case reveals nearly spherical morphology of the porosity. This behaviour is attributed to incomplete bonding of particles due to reduced liquid phase on the deposition surface to fill the interstices. A similar effect is

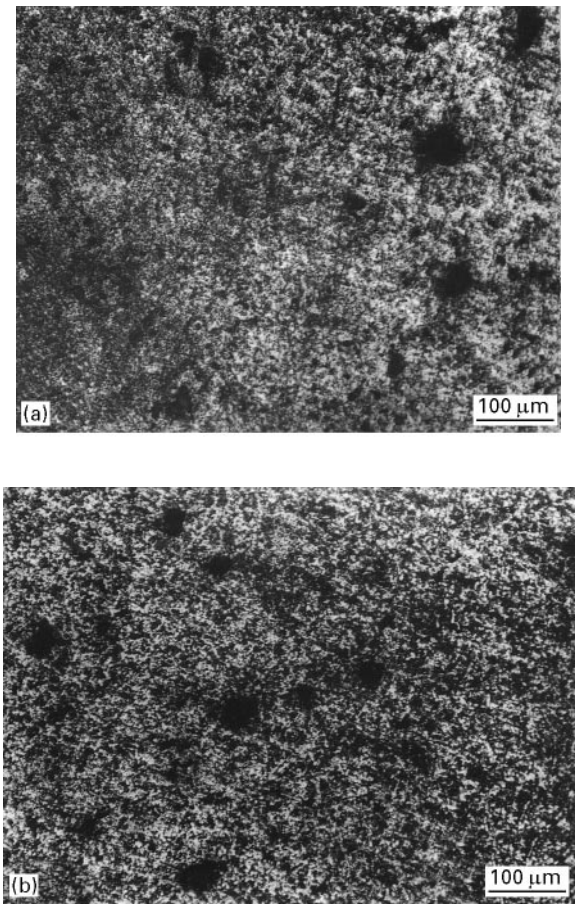

Figure 3 Microstructure of the spray deposit showing (a) irregular shape of pores in the top surface and (b) spherical pores at the centre.

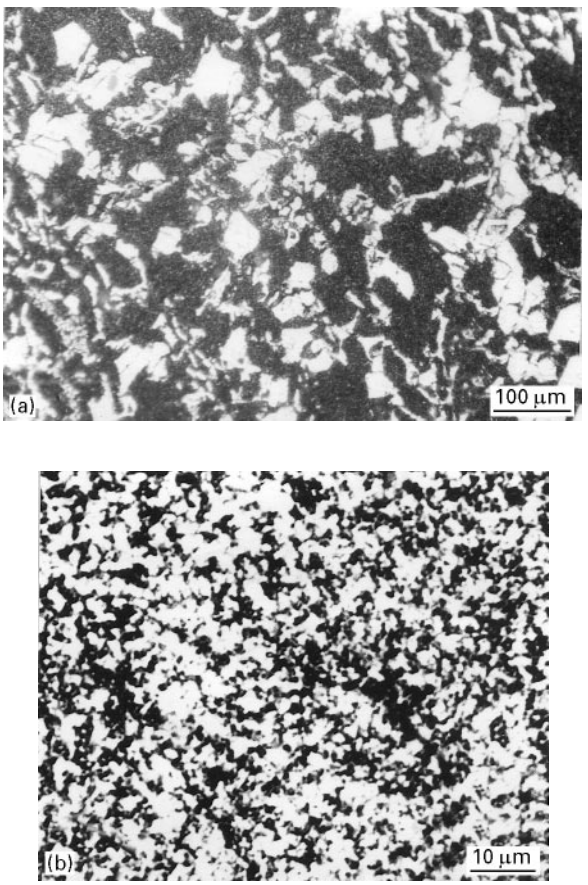

Figure 4 Microstructure showing (a) large size intermetallic phase dispersed in a coarse eutectic matrix of the as-cast alloy and (b) refinement in the microstructure of the spray deposit.

possible in the periphery of the deposit due to decreased size of the droplets in the surface of the spray cone [21] and consequently increasing the solid fraction in the spray. The experimental evidence in the present work illustrates the necessity of using optimum processing conditions to reduce the porosity of the spray deposit.

3.3. Microstructural features

The microstructure of the as-cast alloy as shown in Fig. 4a illustrates dispersion of second phase particles in the matrix of a coarse irregular eutectic. The bulk of the second phase, identified as SnSb intermetallic compound in X-ray diffraction analysis, has characteristic faceted growth morphology and the particle size varies from 50 to 100 μm. The microstructure of a typical spray-formed alloy is shown in Fig. 4b. A noteworthy feature of the spray-formed alloy is the considerable refinement in both the second phase particles and the constituents of the eutectic phases. The size of the second phase particles varies from 3 to 10 μm indicating an order of magnitude in refinement of their size compared to that of the as-cast alloy. The process variables indicated considerable influence on the size, shape and distribution of intermetallic phases of this alloy. At low atomization gas pressure and small nozzle-to-substrate distance, the dispersoid size varied along the through thickness direction of the preform. There was a gradual increase in the size of the second phase particles from the bottom to the top surface of the deposit. The microstructure of the centre of the spray deposit, produced at 1.0 MPa gas pressure and nozzle-to-substrate distance of 0.3 m, is shown in Fig. 5a and b. Similar variation in the microstructure of the deposit, produced at low atomization gas pressure and increased nozzle-to-substrate distances, was observed. However, with an increase in both the gas pressure and nozzle-to-substrate distance, the second phase particles were observed to be relatively smaller and uniformly distributed along the thickness of the deposit. A typical microstructure of the deposit produced at 1.2 MPa gas pressure with 0.4 m nozzle-to-substrate distance is presented in Fig. 6a and b. However, in all cases a considerable uniformity was observed in the distribution of second phase particles and alloying elements throughout the section of the spray deposits.

Fig. 7a and b shows the microstructure of atomized powders. Second phase particles of a distinctly small size are evident. The X-ray diffraction analysis, the details of which is reported elsewhere [32], confirmed the presence of metastable phases, $Cu_{3.3}$ Sb and β″ (CuSn), in atomized powders and Cu_2Sb phase in spray-formed alloy. These phases were not observed in the X-ray diffraction of the as-cast alloy, indicating a considerable departure from the equilibrium solidification condition during atomization and spray-forming processing.

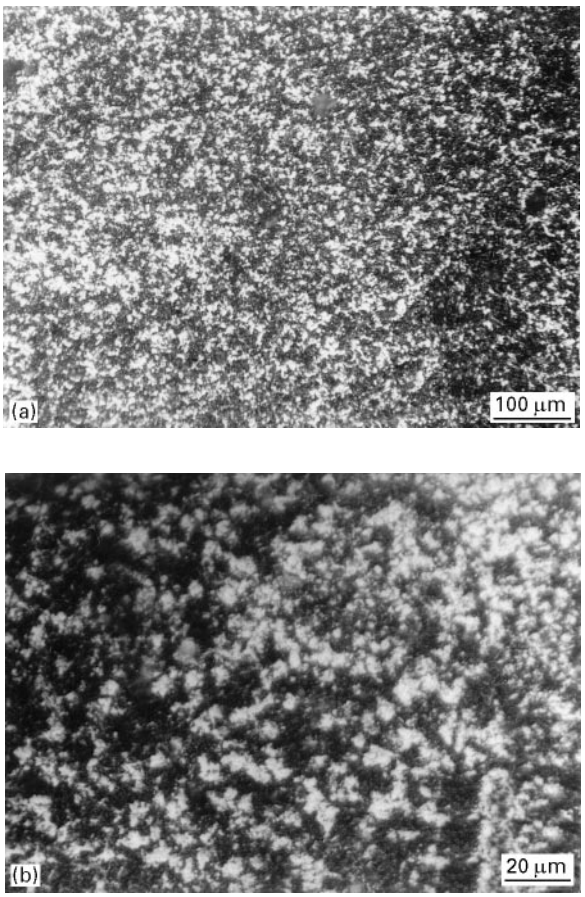

Figure 5 Microstructure of the spray deposit produced at 1.0 MPa gas pressure with a nozzle–substrate distance of 0.3 M showing (a) uniform dispersion of second phase particles and (b) high magnification micrograph of the same region.

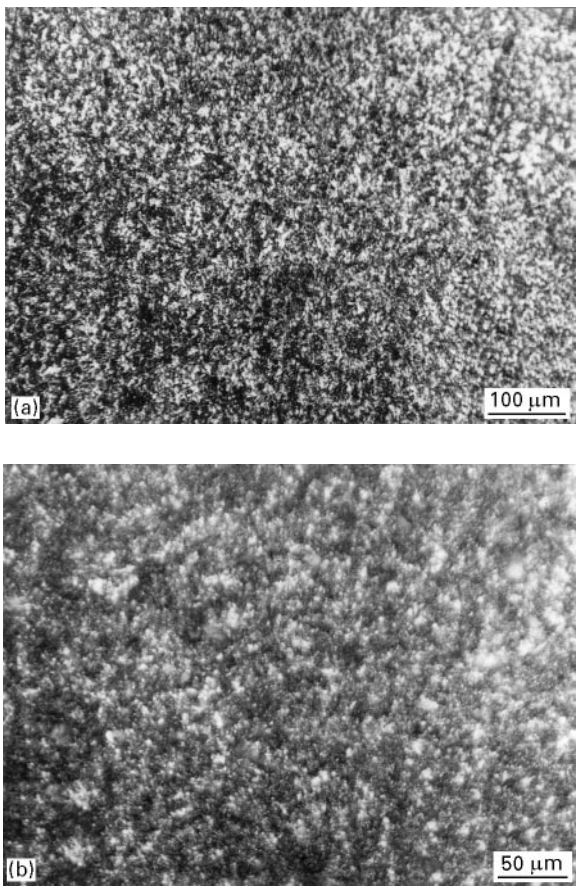

Figure 6 Microstructure of the spray deposit produced at 1.2 MPa gas pressure with 0.4 m nozzle–substrate distance showing (a) refinement in second phase particles and (b) fragmentation of the second phase particles.

An electron probe X-ray microanalysis (EPMA) study was carried out to compare the distribution of alloying elements in both the as-cast and spray-formed alloys. Fig. 8 a to f shows X-ray images of various elements of the as-cast alloy. The X-ray images of the corresponding elements in the spray-formed alloy are presented in Fig. 9a to e. The results indicate considerable chemical homogeneity of the spray-formed alloy compared to that of the as-cast alloy.

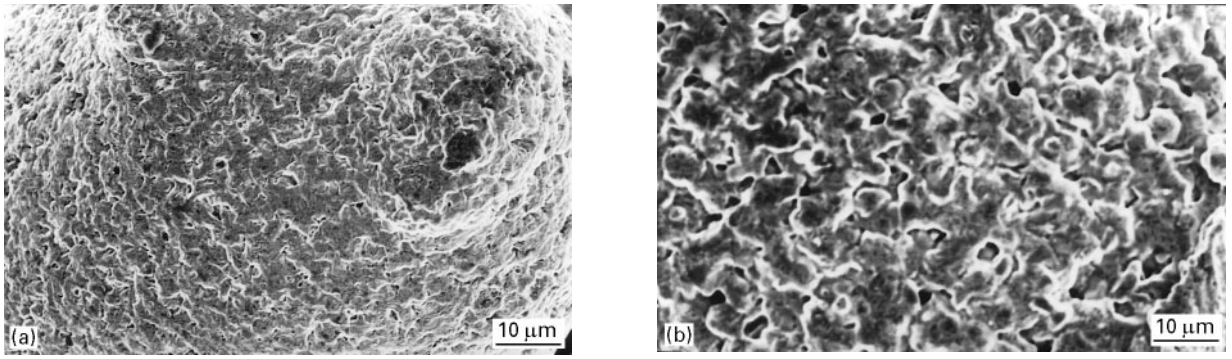

Figure 7 SEM micrograph of atomized powders showing (a) dispersion of submicron size porosity and (b) small size intermetallic phase.

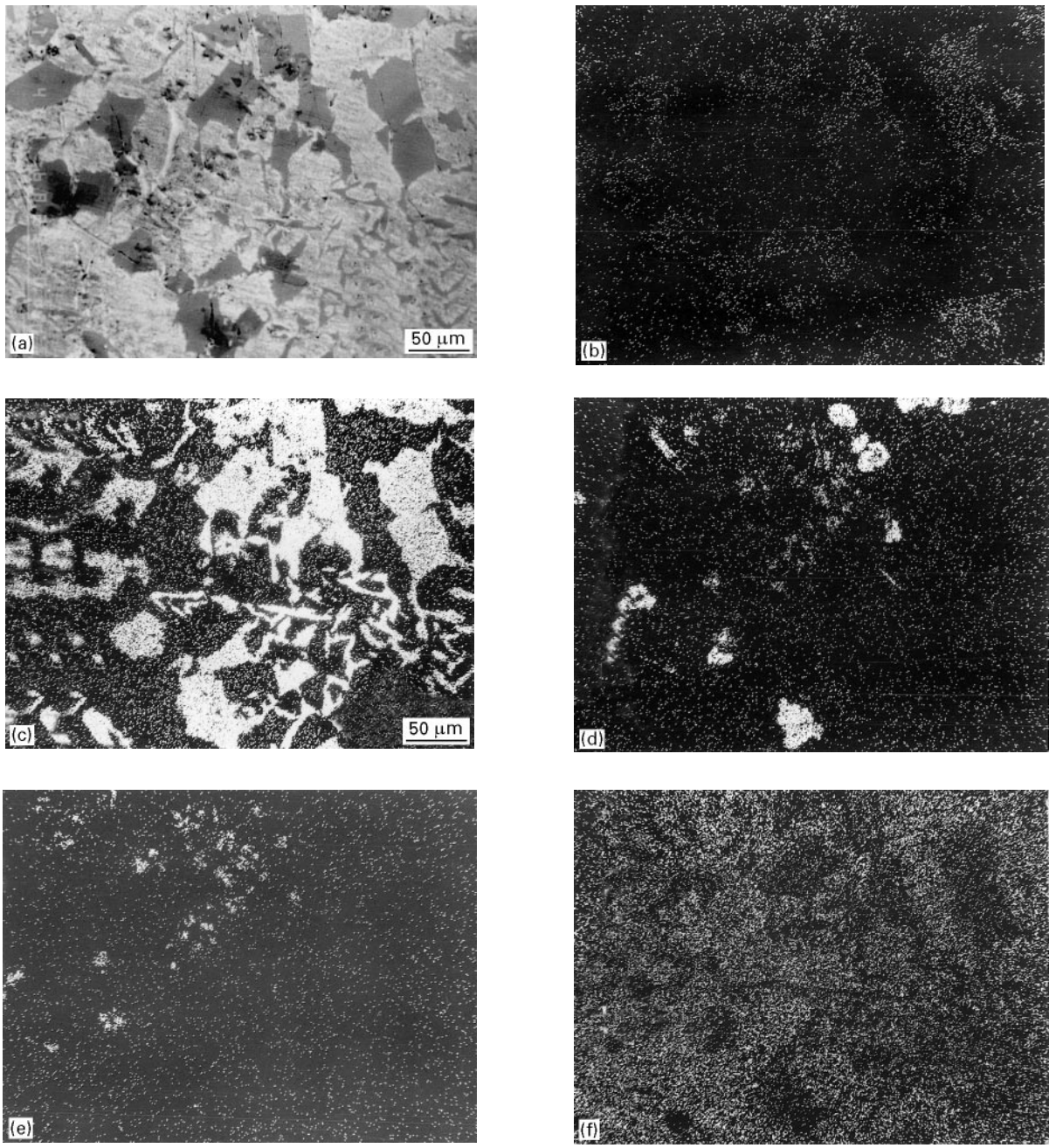

Figure 8 EPMA of the as-cast alloy showing (a) secondary electron image, (b) X-ray image of SnK_{α}, (c) X-ray image of SbK_{α}, (d) X-ray image of CuK_{α}, (e) X-ray image of NiK_{α}, and (f) X-ray image of AsK_{α} radiations.

The above microstructural variation in the as-cast and spray-formed alloys primarily arises due to different solidification conditions prevailing during the process of spray deposition under experimental variables employed in the present work. The microstructural evolution during spray forming is significantly influenced by the droplet dynamics and their thermal state on the deposition surface [5–8]. These are controlled by the process variables employed to atomize the melt and nozzle-to-substrate distance employed during spray forming. An increase in the atomization gas pressure results in refinement in the droplet size in the spray (Fig. 2). Another important variable which influences the droplet size distribution in the spray is the gas-to-metal flow ratio. However, in the confined gas atomization process used in the present work, the melt flow rate is also influenced by the gas flow rate. This effect arises due to the suction pressure created at the tip of the flow tube [26]. As a result it is difficult to control precisely the gas-to-metal flow rate in this process. Consequently small size droplets are subjected to large nucleation undercooling as these are devoided of heterogeneous nucleants [33]. At the same time, increased specific surface area of the droplets gives rise to a relatively higher heat exchange rate at the droplet–gas interface and a high cooling rate of droplets [34]. This effect amounts to an increased fraction of solid in the spray on the deposition surface.

Runs 1 to 3 provide the above condition of spray deposition on a nozzle-to-substrate distance of 0.4 m employed in the present work. Thus, an increased fraction of liquid in Run 1 may generate a large liquid pool on the deposition surface and consequently a slow cooling rate and coarsening in the resultant microstructure of the deposit compared to that in Run 3. The variation in the nozzle to substrate distance at

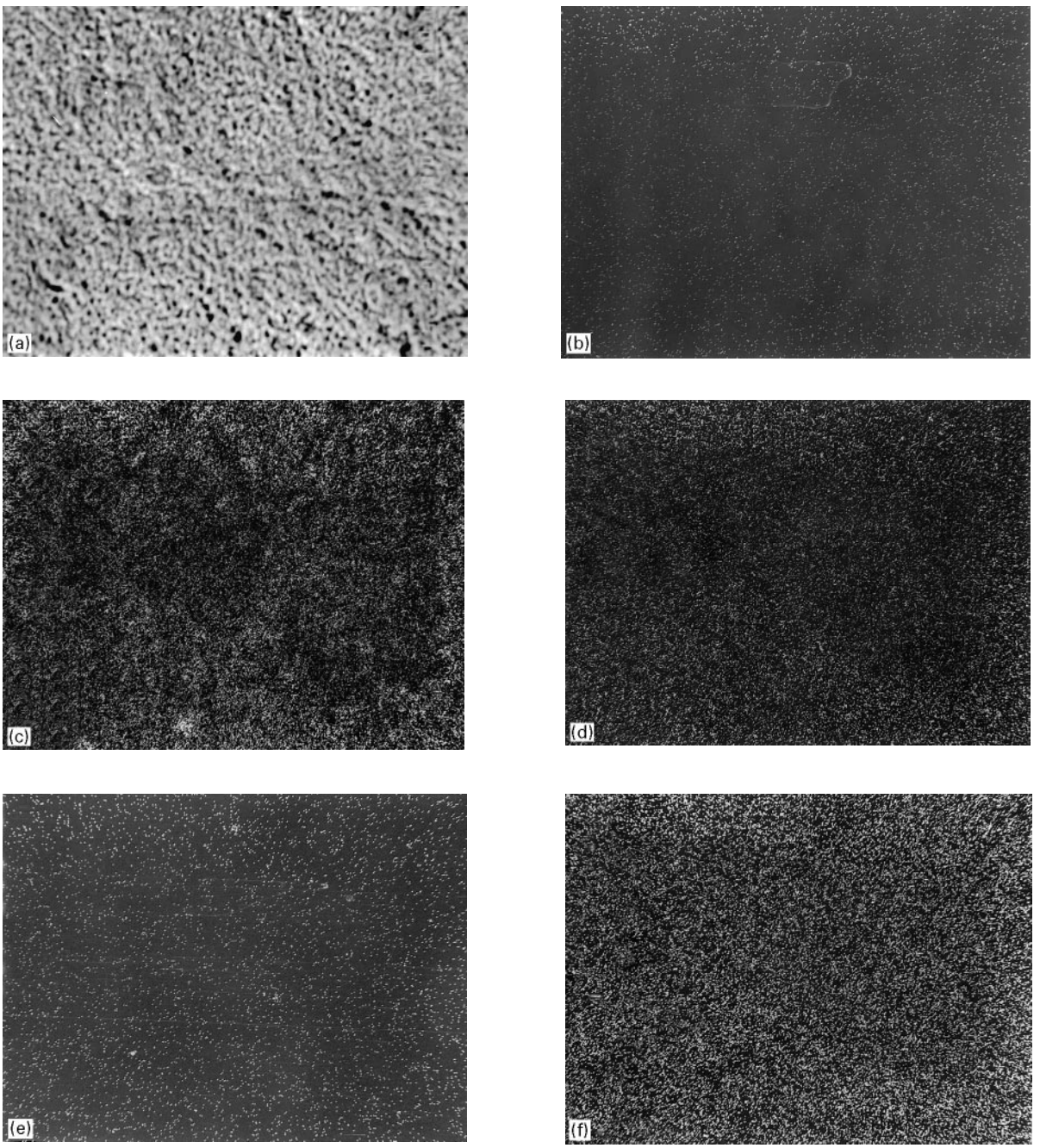

Figure 9 EPMA of the spray-deposited alloy showing (a) secondary electron image, (b) X-ray image of SnK_{α}, (c) X-ray image of SbK_{α}, (d) X-ray image of CuK_{α}, (e) X-ray image of NiK_{α}, and (f) X-ray image of AsK_{α} radiations.

a constant atomization gas pressure in Runs 3 to 5 produce a similar variation in the microstructure of the deposit. In addition, a high gas pressure and low nozzle-to-substrate distance in Run 5 generates maximum porosity with large size pores in the preform. This effect is basically related to whipping of a large liquid pool on the deposition surface by the high-velocity gas stream and large momentum of the droplets generated during this condition of spray deposition.

In an earlier investigation [6] an analysis of heat flow and solidification of droplets during free-flight indicates that the cooling rates, of typical 20 to 150 μm size droplets, are within the range of 10^4 to 10^6 ks^{-1}. The higher value of the cooling rate corresponds to small size droplets. This effect generates metastable phases in atomized powders of this alloy. However, as the wide size range of droplets with their different thermal state impact and coalesce on the deposition surface, the metastable phases are decomposed due to the thermal effect of the large liquid pool. The large momentum transfer by high velocity droplets creates a turbulent fluid flow condition and shearing action of the semi-solid mass on the deposition surface [35].

This behaviour of the spray deposition leads to the fragmentation of partially solidified droplets and a semi-solid mass on the deposition surface to provide enhanced refinement in the size of the intermetallic phases. The coarsening of the second phase is limited due to the high heat exchange rate on the deposition surface by mode of forced convection. In addition, the cooling rate of the semi-solid phase is still sufficient to induce formation of metastable phases in the deposit of this alloy under optimum spray deposition conditions. The observation of Cu_2Sb phase in the spray deposit supports this explanation. The result of the present investigation, thus, indicates that the experimental condition employed in Run 3 is sufficient to minimize porosity and to achieve microstructural homogeneity of this alloy during spray deposition.

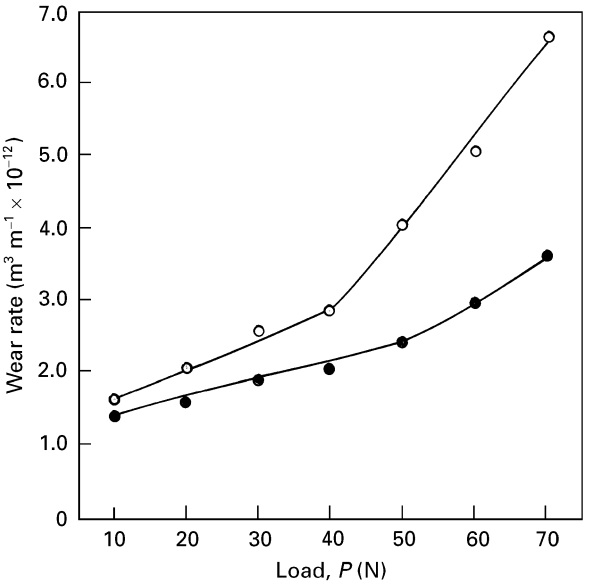

Figure 10 Variation in wear rate with applied load of the as-cast (○) and spray-deposited alloy (●).

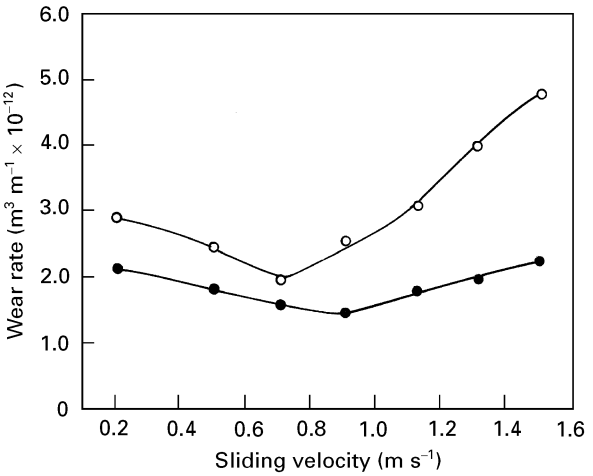

Figure 11 Variation in wear rate with sliding velocity of the as-cast (○) and spray-deposited alloy (●).

3.4. Wear characteristics

Variation in the wear rate of both the as-cast and spray-formed alloys measured as a function of applied load is presented in Fig. 10. In general, the wear rate increases with increasing applied load in both alloys. The wear rate of the as-cast alloy is invariably higher than that of the spray-formed alloy. However, the present result indicates two distinct wear regimes. The first regime consisting of mild wear occurs up to an applied load of 40 N in the as-cast alloy which is extended to a load of 50 N for the spray-formed alloy. The second regime corresponds to the condition of severe wear. In this range of applied load, the wear rate of the as-cast alloy is significantly higher than that of the spray-formed alloy. Fig. 11 shows the effect of sliding velocity on the wear rate of the alloy. It is worthwhile to note that the wear rate initially decreases with increasing sliding velocity. However, a reverse trend is observed beyond a critical sliding velocity. The minimum wear rate of the as-cast alloy is observed at a sliding velocity of 0.70 ms^{-1} compared to 0.90 ms^{-1} for the spray-formed alloy. With further increase in the sliding velocity beyond the critical limit, the wear rate of the as-cast alloy becomes significantly higher than that of the spray-formed alloy.

The different wear characteristics of the spray-formed alloy are related to its microstructural features. The wear behaviour of two phase materials have been reported in several recent investigations [36–38]. In general the size, shape and the nature of the dispersion of the second phase particles in the matrix have been observed to have a strong influence on the wear rate of a wide range of materials. In the present work, the spray-formed alloy exhibits an order of magnitude refinement in the size of the second phase particles with a considerable modification in the microstructure of the eutectic phases. These features of the spray-formed alloy are attributed to strong bonds at the matrix–particle interface due to the decrease in the particle size and the consequent microstructural stability of the alloy under a range of applied loads and sliding velocities.

The dispersoids of the intermetallic phases possess higher hardness values compared to that of the eutectic in this alloy. The low melting constituent of the

eutectic is smeared out on the mating surfaces at an early stage. This effect arises due to the small interparticle spacings of the dispersoids in the spray-formed alloy. Consequently, a thin lubricating film is developed on the surface of the wear test specimen which protects the materials from further wear. The low wear rate of the spray-formed alloy justifies this mechanism. However, the stability of the lubricating film on the specimen surface depends on the applied load and sliding velocity of the mating surfaces. The experimental result indicates that the stability regime of the lubricating film is extended to higher load and sliding velocity in the mild wear regime of the spray-formed alloy. However, as the sliding velocity is further increased instability arises in the continuity of the lubricating film. This is indicated by a significantly high wear rate of the material with further increase in the sliding velocity. Still in this severe wear regime, the spray-formed alloy, owing to the small interparticle spacing of its intermetallics, continues to provide a relatively low wear rate compared to the as-cast alloy.

To summarize, the results of the present investigation reveal a strong influence of the process variables employed during spray forming on the microstructural features and related wear characteristics of the Babbit alloy.

4. Conclusions

The following conclusions are drawn from the results of the present investigation.

1. The process variables during spray forming of a Pb-base Babbit alloy strongly influence the microstructure and porosity of the spray deposits. The process parameters of 1.2 MPa atomization gas pressure and 0.4 m nozzle-to-substrate distance are observed to be the optimum to minimize the porosity and achieve refinement of the intermetallic phases in this alloy.

2. The microstructural homogeneity and formation of metastable phases $Cu_{3.3}Sb$ and β'' (CuSn) in atomized powders and Cu_2Sb spray-formed alloy indicate a considerable departure from the equilibrium solidification condition of this alloy during spray deposition processing.

3. The wear rate of the spray-formed alloy is invariably lower than that of the as-cast alloy. Generally, two distinct regimes corresponding to mild wear and severe wear are observed in both the as-cast and spray-formed alloys investigated under applied loads of 10 to 70 N and sliding velocities of 0.2 to 1.5 ms^{-1}. The mild wear regime is extended to higher load and sliding velocity in spray-formed alloy. The superior wear characteristics of the spray-formed alloy are attributed to the decreased interparticle spacing of the intermetallic phases and modification in the microstructure of the eutectic phases.

Acknowledgements

The authors express their sincere thanks to Professor G.S. Upadhyaya, Department of Materials and Metallurgical Engineering, IIT Kanpur for providing the facility for the porosity measurements. The financial support for this work was provided by the Aeronautics Research and Development Board, Ministry of Defence, Government of India.

References

1. A. R. E. SINGER, *Met. Mater.* **4** (1970) 246.
2. *Idem*, *J. Metals* **100** (1972) 185.
3. R. G. BROOKS, C. MOORE, A. G. LEATHAM and J. S. COOMBS, *Powder Metall.* **20** (1977) 100.
4. P. MATHUR, D. APELIAN and A. LAWLEY, *Acta Metall.* **37** (1989) 429.
5. G. M. GUITIEREZ, E. J. LAVERNIA, G. TRAPAGA, J. SZEKELY and N. J. GRANT, *Met. Trans.* **20A** (1989) 71.
6. S. N. SINGH, S. N. MISHRA and S. N. OJHA, *Steel Res.* **63** (1992) 12.
7. B. P. BEWLAY and B. CANTOR, *J. Mater. Res.* **6** (1991) 1433.
8. P. S. GRANT, B. CANTOR and L. KATGEMAN, *Acta Metall. Mater.* **41** (1993) 3097.
9. E. S. LEE and S. AHN, *ibid.* **42** (1994) 3231.
10. S. N. OJHA, *Bull. Mater. Sci.* **15** (1992) 527.
11. S. N. OJHA, J. N. JHA and S. N. SINGH, *Scripta Metall. Mater.* **25** (1991) 443.
12. E. J. LAVERNIA and N. J. GRANT, *Mater. Sci. Eng.* **98** (1988) 381.
13. P. S. GRANT, *Progress Mater. Sci.* **39** (1995) 497.
14. E. J. LAVERNIA, J. D. AYERS and T. S. SRIVATSEN, *Int. Mater. Rev.* **37** (1992) 1.
15. S. N. OJHA, O. P. PANDEY, B. TRIPATHI, M. KUMAR and C. RAMACHANDRA, *Mater. Trans. JIM* **33** (1992) 519.
16. P. S. GRANT and B. CANTOR, *Acta Metall. Mater.* **43** (1995) 913.
17. S. N. SINGH and S. N. OJHA, *Met. Mater. Processes* **3** (1991) 53.
18. P. S. GRANT, B. CANTOR and L. KATGERMAN, *Acta Metall. Mater.* **41** (1993) 3109.
19. P. S. GRANT, B. CANTOR, S. ROGERS and L. KATGERMAN, *Cast Metals* **3** (1991) 227.
20. S. N. SINGH and S. N. OJHA, *Powder Met. Sci. Technol.* **6** (1995) 25.
21. S. N. OJHA and S. N. SINGH, *J. Mater. Sci. Lett.* **10** (1991) 893.
22. G. H. GEIGER and D. R. POIRIER, "Transport Phenomena in Metallurgy" (Addison-Wesley, Reading, Mass, 1973).
23. G. ARTHUR, *J. Inst. Met.* **84** (1955) 327.
24. E. KLAR and J. W. FESKO, "Metals Handbook", Vol. 7 (American Society for Metals, Metals Park, OH, 1984) p. 25.
25. A. UNAL, *Met. Trans.* **20B** (1989) 61.
26. S. N. SINGH and S. N. OJHA, *Int. J. Rapid Solidification* **7** (1992) 201.
27. J. GRETZINGER and W. R. MARSHAL, *AIChEJ* **7** (1961) 312.
28. W. R. LANE, *Ind. Eng. Chem.* **43** (1951) 1312.
29. A. UNAL, *Mater. Sci. Technol.* **3** (1987) 1029.
30. E. J. LAVERNIA, T. ANDO and N. J. GRANT, in "Rapidly Solidified Materials", edited by P. Lee and R. Carbonara, (American Society for Metals, Metals Park, OH, 1986) p. 29.
31. K. OGATA, E. J. LAVERNIA, G. RAI and N. J. GRANT, *Int. J. Rapid Solidification* **2** (1986) 21.
32. ANISH UPADHYAYA and S. N. OJHA, Proceedings of the International Conference on Powder Metallurgy (APMI, Seattle May 1995) p. 773.
33. R. A. RICKS, NJE ADKINS and T. W. CLYNE, *Powder Met.* **29** (1986) 27.
34. O. P. PANDEY and S. N. OJHA, *Powder Met. Int.* **23** (1991) 9.
35. E. J. LAVERNIA, *Int. J. Rapid Solidification* **5** (1989) 5.
36. A. SATO and R. MEHRABIAN, *Met. Trans.* **7B** (1976) 443.
37. B. C. PAI, SUBRAT RAY, K. V. PRABHAKAR and P. K. ROHATGI, *Mater. Sci. Eng.* **24** (1976) 31.
38. J. P. PATHAK, S. N. TIWARI and S. L. MALHOTRA, *Wear* **112** (1986) 341.

Received 27 February
and accepted 23 October 1996